BeBeC-2020-S05

Spherical acoustical holography using planar microphone arrays

Christof Puhle
GFaI e. V.
Volmerstraße 3, 12489, Berlin, Germany

Abstract

In this paper, we approach the forward exterior problem of spherical acoustical holography, i.e. all sources are contained within a sphere of certain radius, and, using measurements outside this sphere, sound field predictions are obtained from the surface out to the farfield. In this setup, we recently proposed the reconstruction method SIFAH that makes extensive use of spherical numerical integration together with an efficient iteration strategy (see [6]). A characteristic feature of this method is the exact reconstruction of emissions (read: solutions to the Helmholtz equation) up to a certain degree. We now extend this approach to non-spherical measurements, in particular, we allow for the use of planar microphone arrays. Moreover, we require robustness with regards to microphone positioning in this setting. Our considerations include simulations/reconstructions for various source setups including (smoothed) circular spherical cap pistons.

1 Reconstruction of spherical waves

Let $\bar{p} : \mathbb{R}^3 \to \overline{\mathbb{C}}$ be the complex amplitude of a time-harmonic sound pressure field of angular frequency $\omega > 0$ and speed of propagation $c > 0$. By definition, $\bar{p}$ satisfies the Helmholtz equation

$$\frac{\partial^2 \bar{p}}{\partial x^2} + \frac{\partial^2 \bar{p}}{\partial y^2} + \frac{\partial^2 \bar{p}}{\partial z^2} + k^2 \bar{p} = 0, \quad k = \frac{\omega}{c}. \tag{1}$$

Our sign convention for a time-harmonic function is $t \mapsto \exp(i\omega t)$. For example,

$$\bar{p}(x,y,z) = \frac{\exp\left(-ik\sqrt{x^2+y^2+z^2}\right)}{\sqrt{x^2+y^2+z^2}} \tag{2}$$

represents an outgoing spherical wave with source in $(0,0,0)$.

Let $p : [0,\infty] \times [0,\pi] \times [0,2\pi] \to \overline{\mathbb{C}}$ be $\bar{p}$'s representation in spherical coordinates (r,θ,ϕ). Consequently, p satisfies

$$\frac{1}{r^2}\frac{\partial}{\partial r}\left(r^2\frac{\partial p}{\partial r}\right) + \frac{1}{r^2\sin\theta}\frac{\partial}{\partial\theta}\left(\sin\theta\frac{\partial p}{\partial\theta}\right) + \frac{1}{r^2\sin^2\theta}\frac{\partial^2 p}{\partial\phi^2} + k^2 p = 0. \tag{3}$$

Solutions to this equation can be found analytically by assuming that p is separable, i.e. there exist functions $R : [0,\infty] \to \overline{\mathbb{C}}$, $\Theta : [0,\pi] \to \overline{\mathbb{C}}$, $\Phi : [0,2\pi] \to \overline{\mathbb{C}}$ such that

$$p(r,\theta,\phi) = R(r)\cdot\Theta(\theta)\cdot\Phi(\phi). \tag{4}$$

In this case, equation (3) leads to

$$R(r) = A\cdot h_l^{(1)}(kr) + B\cdot h_l^{(2)}(kr) \tag{5}$$

for some constants $A,B \in \mathbb{C}$, $l \in \mathbb{N}_0 = \{0,1,\ldots\}$, and $h_l^{(1)}$, $h_l^{(2)}$ denote the spherical Hankel functions of the first and second kind of degree l, respectively. Moreover, we have

$$\Theta(\theta)\cdot\Phi(\phi) = Y_l^m(\theta,\phi), \tag{6}$$

where $m \in \{-l,-l+1\ldots,l\}$, and Y_l^m is the spherical harmonic of degree l and order m.

We now suppose p is generated in the compact ball of radius $r_0 > 0$ centered at $(0,0,0)$, its complement

$$D = \left\{(x,y,z) \in \mathbb{R}^3 \,:\, r = \sqrt{x^2+y^2+z^2} > r_0\right\} \tag{7}$$

is supposed to be source free. Motivated by Sommerfeld's radiation condition (see [7]), we then assume that (in the area of interest) p is (at least in good approximation) a superposition of the first $(L_0+1)^2$ outgoing separable solutions of (3),

$$p(r,\theta,\phi) = \sum_{l=0}^{L_0}\sum_{m=-l}^{l} B_{lm}\cdot h_l^{(2)}(kr)\cdot Y_l^m(\theta,\phi), \quad B_{lm} \in \mathbb{C}. \tag{8}$$

Based on a measurement of p at the positions

$$(r_i,\theta_i,\phi_i) \in (r_0,\infty] \times [0,\pi] \times [0,2\pi], \quad i = 1,\ldots,N \tag{9}$$

in the source-free region D, we now present an approach to determine/reconstruct the $(L_0+1)^2$ complex numbers $B_{lm} \in \mathbb{C}$ numerically.

1.1 Integration on the sphere

In theory, we can reconstruct the coefficients B_{lm} exactly by integrating over the unit sphere. In fact, for a fixed $r > r_0$, we can write (8) as

$$p^r(\theta,\phi) = \sum_{l=0}^{L_0}\sum_{m=-l}^{l} p_{lm}^r\cdot Y_l^m(\theta,\phi), \tag{10}$$

where

$$p^r(\theta,\phi) = p(r,\theta,\phi), \quad p^r_{lm} = B_{lm} \cdot h^{(2)}_l(kr). \tag{11}$$

Consequently,

$$p^r_{lm} = \int_{S^2} p^r(\theta,\phi) Y^m_l(\theta,\phi)^* d\lambda. \tag{12}$$

One of the most common ways to arrive at a numerical approximation of this integral is by a quadrature, i.e. we approximate it by a weighted sum over a finite collection of points

$$\{(\theta_1,\phi_1),\ldots,(\theta_{N_I},\phi_{N_I})\} \subset [0,\pi]\times[0,2\pi] \tag{13}$$

on the unit sphere:

$$\int_{S^2} f(\theta,\phi) d\lambda \approx \sum_{i=1}^{N_I} w_i \cdot f(\theta_i,\phi_i), \quad w_i \in \mathbb{C}. \tag{14}$$

The theory of quadratures for one-dimensional integrals has a long history and some results can be extended to the two-dimensional case, a noteworthy difference however is that the distribution of points on the unit sphere alone is a non-trivial problem on its own (see [2]).

We now define the finite-dimensional vector space of spherical harmonics up to degree L as

$$\Pi^L = \operatorname{span}\{Y^m_l : 0 \le l \le L, -l \le m \le l\}. \tag{15}$$

Inspecting (10), we therefore have $p^r \in \Pi^{L_0}$ for each $r > r_0$. Since

$$Y^{m_1}_{l_1} \cdot Y^{m_2}_{l_2} \in \Pi^{l_1+l_2}, \tag{16}$$

we later require a quadrature rule for (12) to be exact at least on Π^{2L_0}.

The most basic scheme that ensures exact integration of all spherical harmonics up to a given degree is a Gaussian product, a repeated application of two one-dimensional quadratures. It uses an equally spaced scheme (such as the trapezoidal method) in ϕ and Gauss-Legendre scheme for θ. In order to be exact on Π^L with L odd, we would need $(L+1)/2$ nodes for the θ-integral and $(L+1)$ points for the ϕ-integration, yielding a total of $(L+1)^2/2$ points on the sphere (cf. [2]). A common critique of Gaussian products is the inequality of weights and that the distribution of nodes is clustered around the poles (see Figure 1).

If we impose the requirement that a quadrature has equal weights and is exact for all spherical harmonics up to a given degree, we arrive at spherical designs, which were initially defined in [4] as a problem in algebraic combinatorics. A set of points

$$\{(\theta_1,\phi_1),\ldots,(\theta_{N_I},\phi_{N_I})\} \subset [0,\pi]\times[0,2\pi] \tag{17}$$

is called a spherical L-design if for each $f \in \Pi^L$

$$\int_{S^2} f(\theta,\phi) d\lambda = \frac{4\pi}{N_I} \sum_{i=1}^{N_I} f(\theta_i,\phi_i). \tag{18}$$

Obviously one wants to construct spherical designs with a minimal amount of nodes, and this is

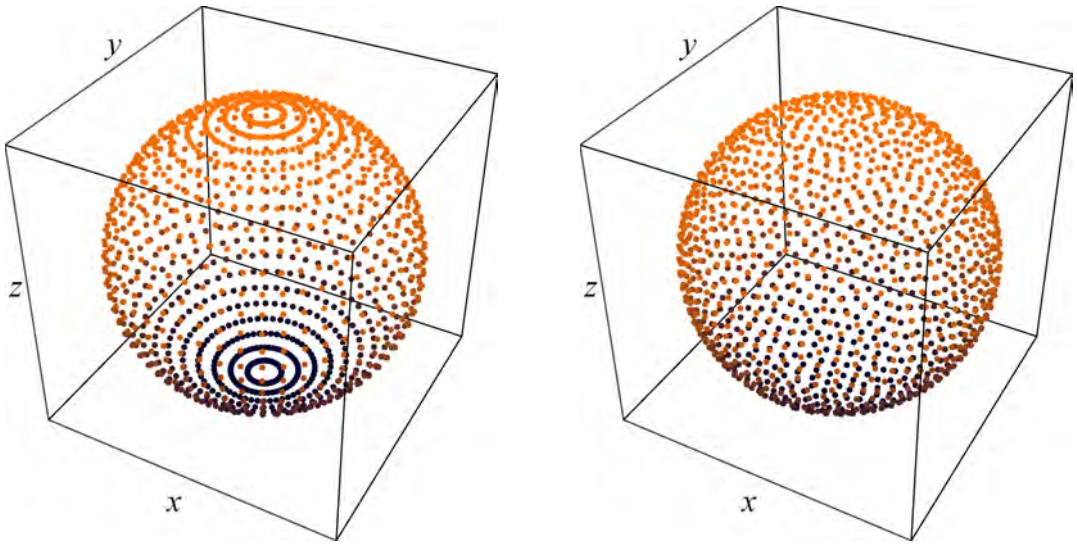

Figure 1: Gaussian product grid of degree $L = 51$ with 1352 nodes (left) and spherical L-design with $L = 51$ and 1328 nodes (right)

a subject of active research (see [1, 3, 5]). For the actual coordinates used in the computations of this paper we refer to [10] with accompanying website [9] containing the datasets of symmetric (i.e. antipodal) spherical L-designs of odd degrees up to $L = 325$. Figure 1 shows an example of degree $L = 51$.

1.2 Reconstruction method SIFAH

For reconstructing the coefficients B_{lm}, we proposed the following in [6]. Choose a spherical L-design

$$\{(\theta_1, \phi_1), \ldots, (\theta_{N_I}, \phi_{N_I})\} \tag{19}$$

and take a measurement of p at the positions

$$(r, \theta_1, \phi_1), \ldots, (r, \theta_{N_I}, \phi_{N_I}), \tag{20}$$

all of which are located on a sphere with radius $r > r_0$ in the source-free region. Then, approximate the coefficients via

$$p^r_{lm} \approx \frac{4\pi}{N_I} \sum_{i=1}^{N_I} p(r, \theta_i, \phi_i) Y_l^m(\theta_i, \phi_i)^*. \tag{21}$$

This approximation is exact, i.e.

$$p^r_{lm} = \frac{4\pi}{N_I} \sum_{i=1}^{N_I} p(r, \theta_i, \phi_i) Y_l^m(\theta_i, \phi_i)^*, \tag{22}$$

for degrees

$$l \leq L - L_0. \tag{23}$$

Consequently, p can be reconstructed completely by taking $L \geq 2L_0$. Conversely, if only an upper bound for L_0 is known, say $L_0 \leq L_{max}$, the above method ensures the exact reconstruction of the first $L - L_{max} + 1$ degrees. For the remainder of this section, we suppose that the degree L of the underlying spherical design is chosen sufficiently large such that (22) holds.

In most real-life applications, it is not possible to measure p in all directions (19) around the sphere. We therefore modified the above method in [6] to render partial measurements possible: Let $p_1^r, \ldots, p_M^r$ be a measurement of p at the so-called active positions

$$(r, \theta_1, \phi_1), \ldots, (r, \theta_M, \phi_M), \tag{24}$$

the corresponding passive positions without any information on p being

$$(r, \theta_{M+1}, \phi_{M+1}), \ldots, (r, \theta_{N_I}, \phi_{N_I}). \tag{25}$$

Using this decomposition, we analyze the right-hand side of (22):

$$p_{lm}^r = \frac{4\pi}{N_I} \sum_{i=1}^{M} p_i^r Y_l^m(\theta_i, \phi_i)^* + \frac{4\pi}{N_I} \sum_{i=M+1}^{N_I} \sum_{\bar{l}=0}^{L_0} \sum_{\bar{m}=-\bar{l}}^{\bar{l}} p_{\bar{l}\bar{m}}^r \cdot Y_{\bar{l}}^{\bar{m}}(\theta_i, \phi_i) Y_l^m(\theta_i, \phi_i)^* \tag{26}$$

for each $l \in \{0, \ldots, L_0\}$, $m \in \{-l, \ldots, l\}$. By introducing

$$x^r = (p_{00}^r, p_{1-1}^r, p_{10}^r, p_{11}^r, \ldots, p_{L_0 L_0}^r) \in \mathbb{C}^{(L_0+1)^2}, \tag{27}$$

$$b^r = (b_{00}^r, b_{1-1}^r, b_{10}^r, b_{11}^r, \ldots, b_{L_0 L_0}^r) \in \mathbb{C}^{(L_0+1)^2}, \quad b_{lm}^r = \frac{4\pi}{N_I} \sum_{i=1}^{M} p_i^r Y_l^m(\theta_i, \phi_i)^*, \tag{28}$$

$$A(x^r) = (a_{00}(x^r), a_{1-1}(x^r), a_{10}(x^r), a_{11}(x^r), \ldots, a_{L_0 L_0}(x^r)) \in \mathbb{C}^{(L_0+1)^2}, \tag{29}$$

$$a_{lm}(x^r) = \frac{4\pi}{N_I} \sum_{i=M+1}^{N_I} \sum_{\bar{l}=0}^{L_0} \sum_{\bar{m}=-\bar{l}}^{\bar{l}} p_{\bar{l}\bar{m}}^r \cdot Y_{\bar{l}}^{\bar{m}}(\theta_i, \phi_i) Y_l^m(\theta_i, \phi_i)^*, \tag{30}$$

we are able to combine the $(L_0+1)^2$ equations of (26) into

$$x^r = b^r + A(x^r) = \mathscr{A}^r(x^r). \tag{31}$$

Consequently, the vector $x^r \in \mathbb{C}^{(L_0+1)^2}$ of coefficients we are trying to reconstruct is a fixed-point of the affine map $\mathscr{A}^r : \mathbb{C}^{(L_0+1)^2} \to \mathbb{C}^{(L_0+1)^2}$ (A is a linear map), and any reconstruction method based on the corresponding fixed-point iteration is called a *SIFAH* method (*Spherical Integration Farfield Acoustical Holography*, see [6]). Using this notation, equation (22) corresponds to the degenerate case of (31), that is $x^r = b^r$ or, equivalently,

$$\mathscr{A}^r(x^r) = b^r = \text{const}. \tag{32}$$

In this case, a SIFAH iteration would converge in just one step to a fixed point regardless of how the starting point $x_0^r \in \mathbb{C}^{(L_0+1)^2}$ is chosen.

1.3 Generalization to non-spherical measurements

We now generalize this approach to allow for active positions with varying radii, e.g. planar measurements.

Firstly, we fix the so-called reconstruction radius $\bar{r} > r_0$, and realize that

$$p_{lm}^{r} = f_l(\bar{r}, r) \cdot p_{lm}^{\bar{r}} \tag{33}$$

for each $r > r_0$, where

$$f_l(\bar{r}, r) = \frac{h_l^{(2)}(kr)}{h_l^{(2)}(k\bar{r})}. \tag{34}$$

Using this extrapolation rule, we can express the pressure on the sphere with radius r in terms of its coefficients at $\bar{r}$:

$$\begin{aligned}\frac{p^r(\theta,\phi)}{f_l(\bar{r},r)} &= \sum_{\bar{m}=-l}^{l} \frac{p_{l\bar{m}}^{r}}{f_l(\bar{r},r)} Y_l^{\bar{m}}(\theta,\phi) + \sum_{\bar{l}=0,\bar{l}\neq l}^{L_0} \sum_{\bar{m}=-\bar{l}}^{\bar{l}} \frac{p_{\bar{l}\bar{m}}^{r}}{f_l(\bar{r},r)} Y_{\bar{l}}^{\bar{m}}(\theta,\phi) \\ &= \sum_{\bar{m}=-l}^{l} p_{l\bar{m}}^{\bar{r}} Y_l^{\bar{m}}(\theta,\phi) + \sum_{\bar{l}=0,\bar{l}\neq l}^{L_0} \sum_{\bar{m}=-\bar{l}}^{\bar{l}} p_{\bar{l}\bar{m}}^{\bar{r}} \frac{f_{\bar{l}}(\bar{r},r)}{f_l(\bar{r},r)} Y_{\bar{l}}^{\bar{m}}(\theta,\phi).\end{aligned} \tag{35}$$

Secondly, we project these spherical functions onto Y_l^m,

$$\begin{aligned}\int_{S^2} \frac{p^r(\theta,\phi)}{f_l(\bar{r},r)} Y_l^m(\theta,\phi)^* d\lambda &= \sum_{\bar{m}=-l}^{l} p_{l\bar{m}}^{\bar{r}} \int_{S^2} Y_l^{\bar{m}}(\theta,\phi) Y_l^m(\theta,\phi)^* d\lambda \\ &\quad + \sum_{\bar{l}=0,\bar{l}\neq l}^{L_0} \sum_{\bar{m}=-\bar{l}}^{\bar{l}} p_{\bar{l}\bar{m}}^{\bar{r}} \int_{S^2} \frac{f_{\bar{l}}(\bar{r},r)}{f_l(\bar{r},r)} Y_{\bar{l}}^{\bar{m}}(\theta,\phi) Y_l^m(\theta,\phi)^* d\lambda \\ &= p_{lm}^{\bar{r}} + \sum_{\bar{l}=0,\bar{l}\neq l}^{L_0} \sum_{\bar{m}=-\bar{l}}^{\bar{l}} p_{\bar{l}\bar{m}}^{\bar{r}} \int_{S^2} \frac{f_{\bar{l}}(\bar{r},r)}{f_l(\bar{r},r)} Y_{\bar{l}}^{\bar{m}}(\theta,\phi) Y_l^m(\theta,\phi)^* d\lambda.\end{aligned} \tag{36}$$

This formula may seem silly at first since the left-hand side equals $p_{lm}^{\bar{r}}$ by definition and the second term on the right-hand side obviously equals zero. However, a completely analogous consideration shows that this formula still holds when moving on to varying radii $r \to r(\theta,\phi)$, with r being at least piecewise continuous on the sphere:

$$\begin{aligned}\int_{S^2} \frac{p(r(\theta,\phi),\theta,\phi)}{f_l(\bar{r},r(\theta,\phi))} Y_l^m(\theta,\phi)^* d\lambda &= p_{lm}^{\bar{r}} \\ &\quad + \sum_{\bar{l}=0,\bar{l}\neq l}^{L_0} \sum_{\bar{m}=-\bar{l}}^{\bar{l}} p_{\bar{l}\bar{m}}^{\bar{r}} \int_{S^2} \frac{f_{\bar{l}}(\bar{r},r(\theta,\phi))}{f_l(\bar{r},r(\theta,\phi))} Y_{\bar{l}}^{\bar{m}}(\theta,\phi) Y_l^m(\theta,\phi)^* d\lambda.\end{aligned} \tag{37}$$

Now, from this general point of view, the second term on the right-hand does not necessarily vanish, but quantifies how much the left-hand side deviates from the coefficient $p_{lm}^{\bar{r}}$.

In the next step, we analyze both integrals of (37) numerically using our spherical design (19), again projected and decomposed into active and passive positions (cf. (24), (25)). We allow the radius of the former to vary, but the latter are fixed to lie on the reconstruction sphere. More specifically, the active positions are

$$(r(\theta_1,\phi_1),\theta_1,\phi_1),\ldots,(r(\theta_M,\phi_M),\theta_M,\phi_M)=(r_1,\theta_1,\phi_1),\ldots,(r_M,\theta_M,\phi_M), \tag{38}$$

the passive positions being

$$(r(\theta_{M+1},\phi_{M+1}),\theta_{M+1},\phi_{M+1}),\ldots,(r(\theta_{N_I},\phi_{N_I}),\theta_{N_I},\phi_M)=(\bar{r},\theta_{M+1},\phi_{M+1}),\ldots,(\bar{r},\theta_{N_I},\phi_{N_I}), \tag{39}$$

and $p_1,\ldots,p_M$ is a measurement of p at the active positions, i.e.

$$p_i = p(r_i,\theta_i,\phi_i). \tag{40}$$

As before, we suppose that the underlying degree L is chosen sufficiently large in order to work with equalities. On the one hand, we have

$$\begin{aligned}\int_{S^2}\frac{p(r(\theta,\phi),\theta,\phi)}{f_l(\bar{r},r(\theta,\phi))}Y_l^m(\theta,\phi)^*d\lambda &= \frac{4\pi}{N_I}\sum_{i=1}^{N_I}\frac{p(r(\theta_i,\phi_i),\theta_i,\phi_i)}{f_l(\bar{r},r(\theta_i,\phi_i))}Y_l^m(\theta_i,\phi_i)^*\\ &= \frac{4\pi}{N_I}\sum_{i=1}^{M}\frac{p_i}{f_l(\bar{r},r_i)}Y_l^m(\theta_i,\phi_i)^*\\ &\quad+\frac{4\pi}{N_I}\sum_{i=M+1}^{N_I}p^{\bar{r}}(\theta_i,\phi_i)Y_l^m(\theta_i,\phi_i)^*\\ &= \frac{4\pi}{N_I}\sum_{i=1}^{M}\frac{p_i}{f_l(\bar{r},r_i)}Y_l^m(\theta_i,\phi_i)^*\\ &\quad+\frac{4\pi}{N_I}\sum_{i=M+1}^{N_I}\sum_{\bar{l}=0}^{L_0}\sum_{\bar{m}=-\bar{l}}^{\bar{l}}p_{\bar{l}\bar{m}}^{\bar{r}}\cdot Y_{\bar{l}}^{\bar{m}}(\theta_i,\phi_i)Y_l^m(\theta_i,\phi_i)^*.\end{aligned} \tag{41}$$

On the other hand, when investigating the right-hand side of (37) in this manner, we conclude

$$\begin{aligned}\int_{S^2}\frac{p(r(\theta,\phi),\theta,\phi)}{f_l(\bar{r},r(\theta,\phi))}Y_l^m(\theta,\phi)^*d\lambda &= p_{lm}^{\bar{r}}\\ &\quad+\frac{4\pi}{N_I}\sum_{i=1}^{M}\sum_{\bar{l}=0,\bar{l}\neq l}^{L_0}\sum_{\bar{m}=-\bar{l}}^{\bar{l}}p_{\bar{l}\bar{m}}^{\bar{r}}\frac{f_{\bar{l}}(\bar{r},r_i)}{f_l(\bar{r},r_i)}Y_{\bar{l}}^{\bar{m}}(\theta_i,\phi_i)Y_l^m(\theta_i,\phi_i)^*\\ &\quad+\frac{4\pi}{N_I}\sum_{i=M+1}^{N_I}\sum_{\bar{l}=0,\bar{l}\neq l}^{L_0}\sum_{\bar{m}=-\bar{l}}^{\bar{l}}p_{\bar{l}\bar{m}}^{\bar{r}}Y_{\bar{l}}^{\bar{m}}(\theta_i,\phi_i)Y_l^m(\theta_i,\phi_i)^*.\end{aligned} \tag{42}$$

Finally, we combine (41) and (42) into

$$\begin{aligned} p_{lm}^{\bar{r}} = &\frac{4\pi}{N_I}\sum_{i=1}^{M}\frac{p_i}{f_l(\bar{r},r_i)}Y_l^m(\theta_i,\phi_i)^* \\ &+\frac{4\pi}{N_I}\sum_{i=M+1}^{N_I}\sum_{\bar{m}=-l}^{l} p_{l\bar{m}}^{\bar{r}}\cdot Y_l^{\bar{m}}(\theta_i,\phi_i)Y_l^m(\theta_i,\phi_i)^* \\ &-\frac{4\pi}{N_I}\sum_{i=1}^{M}\sum_{\bar{l}=0,\bar{l}\neq l}^{L_0}\sum_{\bar{m}=-\bar{l}}^{\bar{l}} p_{\bar{l}\bar{m}}^{\bar{r}}\frac{f_{\bar{l}}(\bar{r},r_i)}{f_l(\bar{r},r_i)}Y_{\bar{l}}^{\bar{m}}(\theta_i,\phi_i)Y_l^m(\theta_i,\phi_i)^*. \end{aligned} \tag{43}$$

As in the last section, this gives rise to a fixed point equation for the coefficient vector

$$x^{\bar{r}} = (p_{00}^{\bar{r}}, p_{1-1}^{\bar{r}}, p_{10}^{\bar{r}}, p_{11}^{\bar{r}}, \ldots, p_{L_0L_0}^{\bar{r}}) \in \mathbb{C}^{(L_0+1)^2} \tag{44}$$

of p at the reconstruction radius $\bar{r}$. Since this generalizes (26), or equivalently (31), we will call any corresponding fixed-point method SIFAH as well.

2 Simulation of spherical cap pistons

A vibrating spherical cap piston with aperture angle $\alpha \in (0, 2\pi]$ centered on the north pole of an otherwise rigid sphere with radius r_0 can be described by its surface velocity

$$v^\alpha : [0,\pi]\times[0,2\pi] \to \mathbb{R}, \quad v^\alpha(\theta,\phi) = V\cdot a^\alpha(\theta,\phi), \quad V\in\mathbb{R}, \tag{45}$$

the corresponding aperture function $a^\alpha : [0,\pi]\times[0,2\pi]\to\mathbb{R}$ is given by

$$a^\alpha(\theta,\phi) = 1 - H\left(\theta - \frac{\alpha}{2}\right), \quad H(x) = \begin{cases} 0 & x<0 \\ 1 & x\geq 0 \end{cases}. \tag{46}$$

The spherical wave spectrum of v^α,

$$v^\alpha(\theta,\phi) = \sum_{l=0}^{\infty}\sum_{m=-l}^{l} v_{lm}^\alpha\cdot Y_l^m(\theta,\phi), \tag{47}$$

can be computed via

$$v_{lm}^\alpha = V\delta_{m0}\sqrt{(2l+1)\pi}\int_{\cos\left(\frac{\alpha}{2}\right)}^{1} P_l^0(x)dx. \tag{48}$$

Rotating the spherical cap to be centered in the direction $(\tilde{\theta},\tilde{\phi})$ results in

$$\tilde{v}_{lm}^\alpha = \sqrt{\frac{4\pi}{2l+1}}Y_l^m(\tilde{\theta},\tilde{\phi})^*\cdot v_{lm}^\alpha, \tag{49}$$

respectively. Finally, the radiated pressure in the source-free region is completely determined by the surface velocity spectrum (see for example [8]):

$$p_{v^\alpha}(r,\theta,\phi) = -i\rho_0 c \sum_{l=0}^{\infty} \sum_{m=-l}^{l} \frac{h_l^{(2)}(kr)}{h_l^{(2)\prime}(kr_0)} v_{lm}^{\alpha} \cdot Y_l^m(\theta,\phi). \tag{50}$$

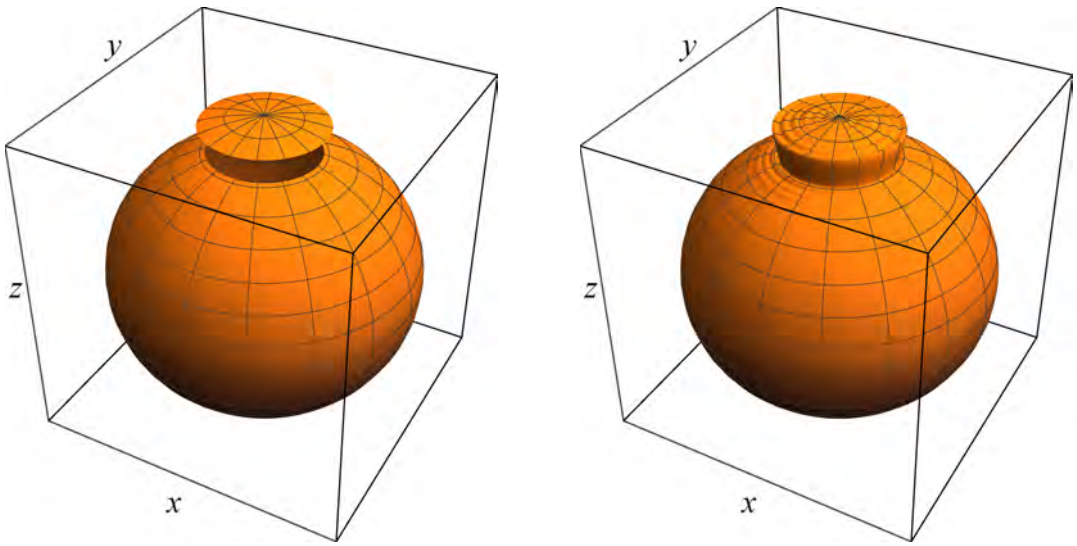

Figure 2: Radial plot of v^α for $\alpha = 40°$ (left) and its spherical wave expansion up to degree $L = 120$ (right)

2.1 Smooth spherical pistons

As hinted at in Figure 2, most of the higher degrees in the expansion (47) of v^α are present to form the discontinuity at the boundary of the spherical cap. In order to avoid this discontinuity, we also introduce a smooth one-parameter family of spherical pistons with surface velocity

$$w^\alpha : [0,\pi] \times [0,2\pi] \to \mathbb{R}, \quad w^\alpha(\theta,\phi) = V \cdot \exp\left(-\frac{(1-\cos(\theta))^2}{\left(1-\cos\left(\frac{\alpha}{2}\right)\right)^2} \right). \tag{51}$$

Again, we will call α the aperture angle of this piston, but now, when varying θ from 0 to $\alpha/2$, the particle velocity smoothly changes from V to V/e. As before, the spherical wave spectrum of w^α can be determined by one-dimensional integration (cf. Figure 3 and Figure 4):

$$w_{lm}^{\alpha} = V \delta_{m0} \sqrt{(2l+1)\pi} \int_{-1}^{1} P_l^0(x) \exp\left(-\frac{(1-x)^2}{\left(1-\cos\left(\frac{\alpha}{2}\right)\right)^2} \right) dx. \tag{52}$$

Moreover, transformation rule (49) also holds for the coefficients w_{lm}^{α} when rotating the smooth spherical piston to be centered in the direction $(\tilde{\theta},\tilde{\phi})$, and the radiated sound pressure p_{w^α}

corresponding to w^α can be computed in complete analogy to (50).

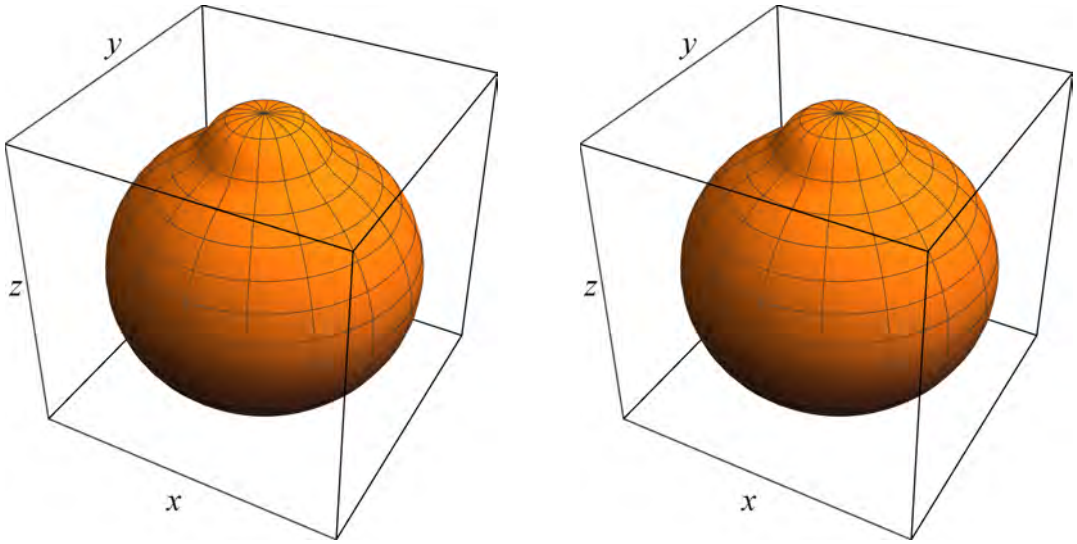

Figure 3: Radial plot of w^α for $\alpha = 40^\circ$ (left) and its spherical wave expansion up to degree $L = 120$ (right)

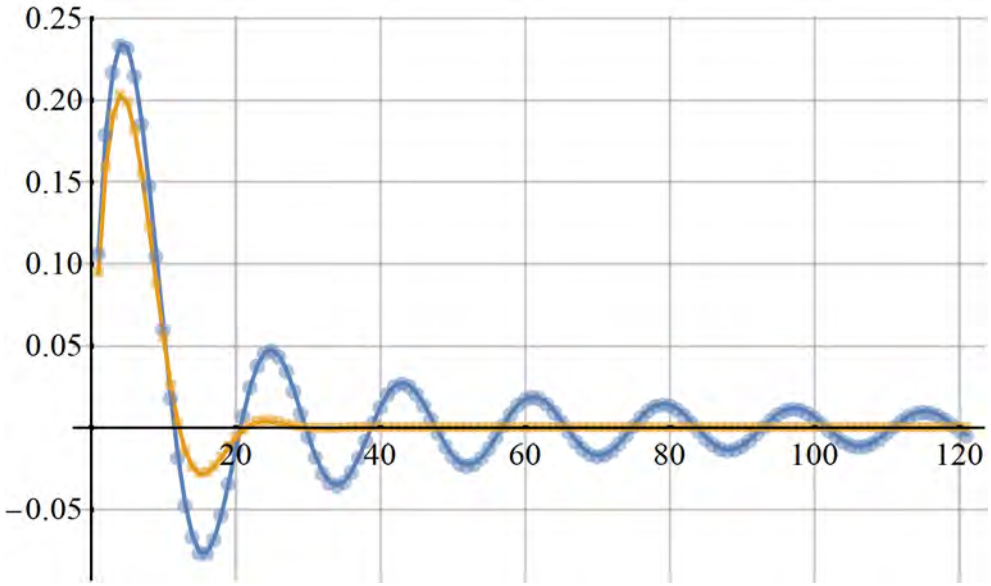

Figure 4: Coefficients v_{l0}^α (blue circles) and w_{l0}^α (yellow boxes) for $\alpha = 40^\circ$ in units of V

3 Results

To exemplify the capabilities of SIFAH, we now reconstruct the simulated sound pressure field generated by one or more (smooth) spherical pistons vibrating at $r_0 = 2.5\,\mathrm{m}$. The simulation

degree is 120 (cf. Figures 2, 3 and 4). In order to determine/reconstruct degrees up to $L_0 = 35$, we pick the symmetric spherical L-design with $L = 71$ listed in [9] and choose $\bar{r} = 4\,\mathrm{m}$ as reconstruction radius. The simulated sound pressure field is measured using three planar matrix-shaped microphone arrays: front and rear array each consist of 9×11 microphones, they are of dimension $2.4\,\mathrm{m} \times 3.0\,\mathrm{m}$, the center array uses 17×11 microphones in a plane of $4.8\,\mathrm{m} \times 3.0\,\mathrm{m}$, resulting in a total of 385 microphones (see Figure 5).

To employ the SIFAH method, we decompose the chosen spherical design into $M = 406$ active and 2152 passive directions, the former being those, whose projection lie in one of the measurement planes of the array. Since none of these projected positions (r_i, θ_i, ϕ_i) coincides with a microphone position, we have – in addition to 28 dB of noise – only approximate knowledge of the $p_1, \ldots, p_M$ in the fixed-point equations (43).

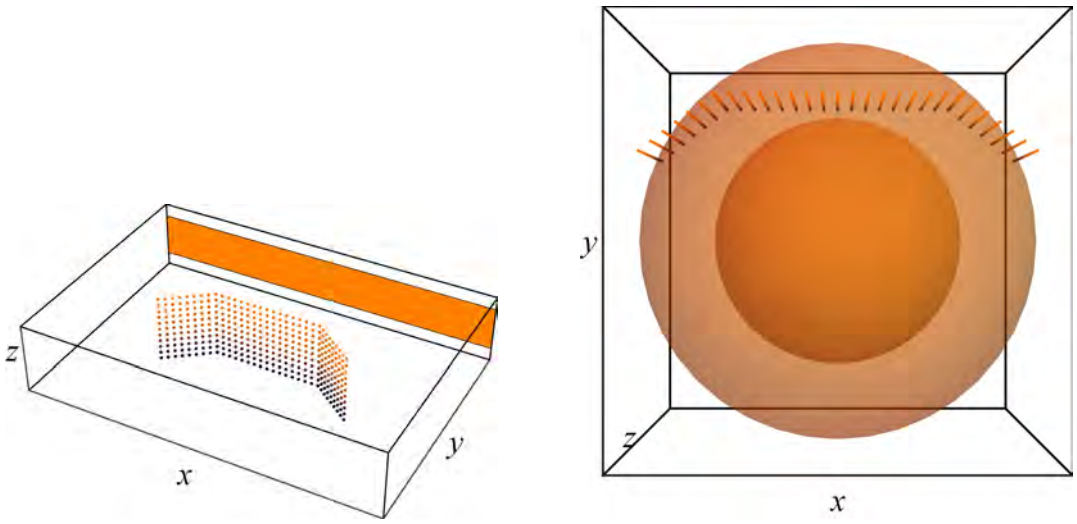

Figure 5: Microphone array and reconstruction plane (left) and vibration and reconstruction radius in relation to array dimensions (right)

The start vector of pressure coefficients at reconstruction radius $\bar{r}$ in the SIFAH fixed-point iteration is chosen as

$$x_0^{\bar{r}} = 0 \in \mathbb{C}^{(L_0+1)^2}, \tag{53}$$

the maximal number of iteration steps is 50. Finally, the resulting vector of coefficients is used to reconstruct the sound pressure in the plane defined by (cf. Figure 5)

$$(x, y, z) \in [-8\,\mathrm{m}, 8\,\mathrm{m}] \times \{8\,\mathrm{m}\} \times [-1\,\mathrm{m}, 1\,\mathrm{m}]. \tag{54}$$

In the first example, we simulate a spherical cap piston with aperture angle $\alpha = 90^\circ$ centered in the direction $(0, 1, 0)$ (see section 2). For each of the considered frequencies $f = 250\,\mathrm{Hz}$, 500 Hz, 1000 Hz, both the simulated and the reconstructed pressures clearly exhibit the limited number of simulation degrees (see Figures 6, 7 and 8).

Using the same aperture angle, direction and frequencies, we then simulate a smooth spherical piston as our second example (see subsection 2.1). Now, simulation and reconstruction are in excellent agreement with each other (see Figures 9, 10 and 11). Moreover, given the limited

number of simulation degrees, this one-parameter family of pistons seems to be well-suited for modeling directional sources.

Therefore, the third and final example consists of four smooth spherical pistons (each of the same maximal surface velocity V), the directions and aperture angles of which are

$$\begin{aligned}(\theta_1,\phi_1,\alpha_1) &= (80^\circ,110^\circ,20^\circ), & (\theta_2,\phi_2,\alpha_2) &= (100^\circ,30^\circ,100^\circ),\\ (\theta_3,\phi_3,\alpha_3) &= (95^\circ,120^\circ,40^\circ), & (\theta_4,\phi_4,\alpha_4) &= (100^\circ,90^\circ,15^\circ).\end{aligned} \tag{55}$$

The frequencies under consideration are $f = 250\,\mathrm{Hz}$, $1000\,\mathrm{Hz}$, $4000\,\mathrm{Hz}$. As the linear nature of the approach suggests, the SIFAH method successfully reconstructs the sound pressure field for this superposition of directional sources (see Figures 12, 13 and 14).

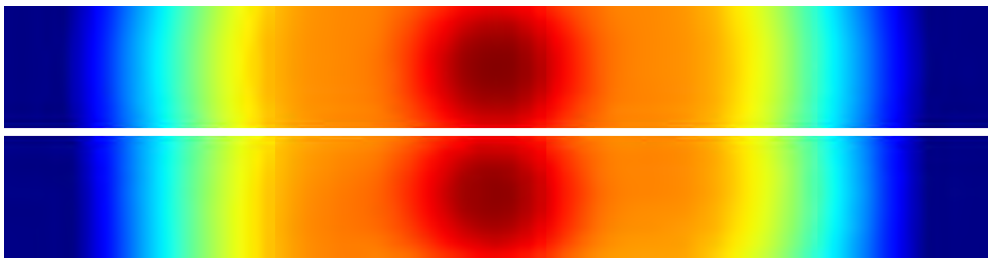

Figure 6: Pressure magnitude (12 dB), single spherical cap piston, $f = 250\,Hz$, simulation of degree 120 (top) and SIFAH reconstruction of degree 35 (bottom)

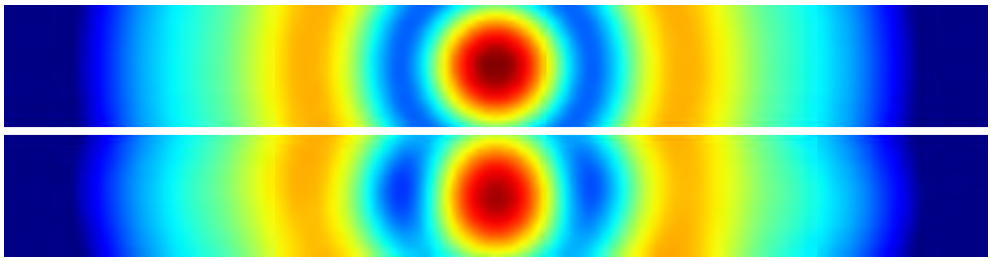

Figure 7: Pressure magnitude (12 dB), single spherical cap piston, $f = 500\,Hz$, simulation of degree 120 (top) and SIFAH reconstruction of degree 35 (bottom)

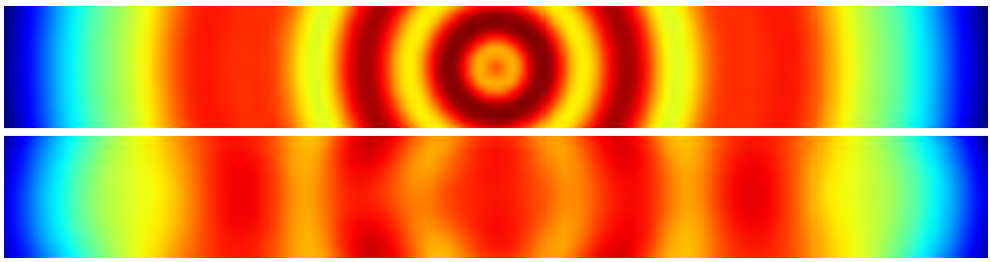

Figure 8: Pressure magnitude (12 dB), single spherical cap piston, $f = 1000\,Hz$, simulation of degree 120 (top) and SIFAH reconstruction of degree 35 (bottom)

Figure 9: Pressure magnitude (12 dB), single smooth spherical piston, $f = 250\,Hz$, simulation of degree 120 (top) and SIFAH reconstruction of degree 35 (bottom)

Figure 10: Pressure magnitude (12 dB), single smooth spherical piston, $f = 500\,Hz$, simulation of degree 120 (top) and SIFAH reconstruction of degree 35 (bottom)

Figure 11: Pressure magnitude (12 dB), single smooth spherical piston, $f = 1000\,Hz$, simulation of degree 120 (top) and SIFAH reconstruction of degree 35 (bottom)

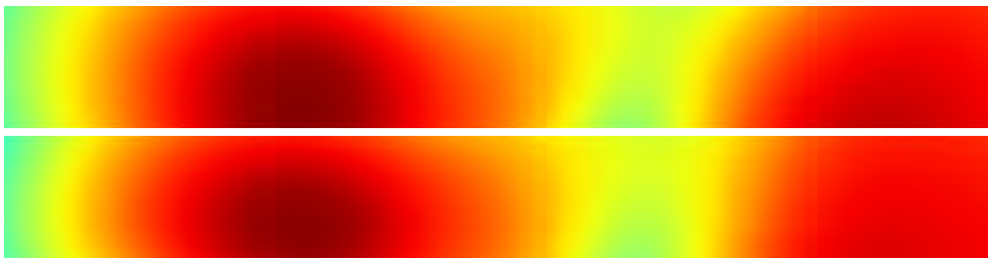

Figure 12: Pressure magnitude (12 dB), multiple smooth spherical pistons, $f = 250\,Hz$, simulation of degree 120 (top) and SIFAH reconstruction of degree 35 (bottom)

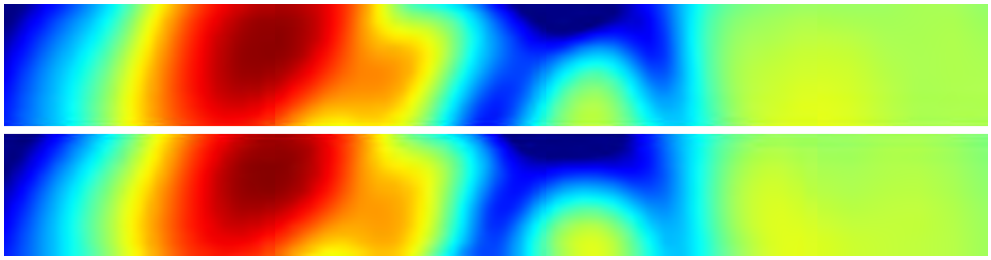

Figure 13: Pressure magnitude (12 dB), multiple smooth spherical pistons, $f = 1000\,Hz$, simulation of degree 120 (top) and SIFAH reconstruction of degree 35 (bottom)

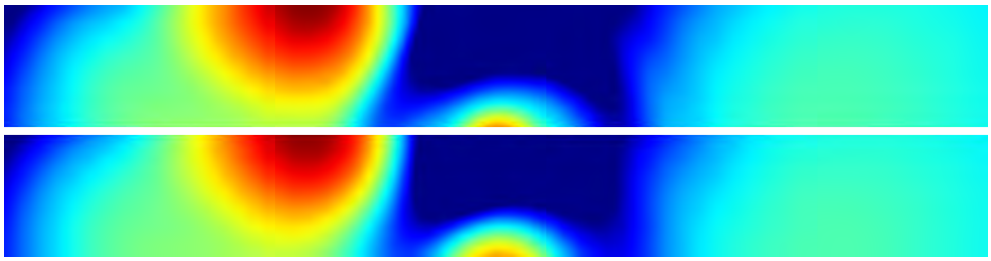

Figure 14: Pressure magnitude (12 dB), multiple smooth spherical pistons, $f = 4000\,Hz$, simulation of degree 120 (top) and SIFAH reconstruction of degree 35 (bottom)

4 Acknowledgements

This research work has been funded by German Federal Ministry for Economic Affairs and Energy (Bundesministerium für Wirtschaft und Energie BMWi) under project *SopraHM* registration number 49MF180103.

References

[1] E. Bannai. "A survey on spherical designs and algebraic combinatorics on spheres." *European Journal of Combinatorics*, 30, 1392–1425, 2009.

[2] C. Beentjes. "Quadrature on a spherical surface." Technical report, Mathematical Institute, University of Oxford, Oxford, UK, 2015.

[3] J. Brauchart and P. Grabner. "Distributing many points on spheres: Minimal energy and designs." *Journal of Complexity*, 31, 293–326, 2015.

[4] P. Delsarte, J. Goethals, and J. Seidel. "Spherical codes and designs." *Geometriae Dedicata*, 58, 363–388, 1977.

[5] R. Hardin and N. Sloane. "Mclarens improved snub cube and other new spherical designs in three dimensions." *Discrete & Computational Geometry*, 15, 429–441, 1996.

[6] C. Puhle. "Spherical integration in acoustical holography." In *Proceedings of 48th International Congress and Exposition on Noise Control Engineering, 16-19 June, Madrid, Spain*. 2019.

[7] A. Sommerfeld. *Partial differential equations in physics*, volume 1 of *Pure and Applied Mathematics*. Academic Press, New York, 1949.

[8] E. Williams. *Fourier acoustics: sound radiation and nearfield acoustical holography*. Academic Press, 1999.

[9] R. Womersley. "Symmetric spherical designs on the sphere $\mathbb{S}^2$ with good geometric properties." URL `http://web.maths.unsw.edu.au/~rsw/Sphere/EffSphDes/`.

[10] R. Womersley. "Efficient spherical designs with good geometric properties." In *Contemporary Computational Mathematics - A Celebration of the 80th Birthday of Ian Sloan* (edited by J. Dick, F. Kuo, and H. Woźniakowski), pages 1243–1285. Springer, 2018.